Redox Biology 37 (2020) 101688

Contents lists available at ScienceDirect

Redox Biology

journal homepage: www.elsevier.com/locate/redox

Research Paper

Myeloid FBW7 deficiency disrupts redox homeostasis and aggravates dietary-induced insulin resistance

Cheng Wang [a,b,*,1], Yuelin Chao [c,1], Wenjing Xu [a], Zhaoyu Liu [d], Huan Wang [e], Kai Huang [a]

[a] Clinic Center of Human Gene Research, Union Hospital, Tongji Medical College, Huazhong University of Science and Technology, Wuhan, China
[b] Department of Rheumatology, Union Hospital, Tongji Medical College, Huazhong University of Science and Technology, Wuhan, China
[c] Department of Cardiology, Nanjing First Hospital, Nanjing Medical University, Nanjing, China
[d] Department of Cardiology, Sun Yat-sen Memorial Hospital, Sun Yat-sen University, Guangzhou, China
[e] Department of Cardiology, The First Affiliated Hospital, Cardiovascular Institute, Harbin Medical University, Harbin, China

ARTICLE INFO

Keywords:
Macrophage
Oxidative stress
Insulin resistance
Inflammasome
Ubiquitination

ABSTRACT

The E3 ubiquitin ligase FBW7 plays critical roles in multiple pathological and physiological processes. Here, we report that after high-fat diet (HFD) feeding for 16 weeks, myeloid-specific FBW7-deficient mice demonstrate increased redox stress, inflammatory responses and insulin resistance. Macrophages activation under FBW7 deficiency decreases substrate flux through the pentose phosphate pathway (PPP) to produce less equivalents (NADPH and GSH) and aggravate the generation of intracellular reactive oxygen species (ROS) in macrophages, thereby over-activating proinflammatory reaction. Mechanistically, we identify that pyruvate kinase muscle isozyme M2 (PKM2) is a new bona fide ubiquitin substrate of SCF^{FBW7}. While challenged with HFD stress, pharmacological inhibition of PKM2 protects FBW7-deficient macrophages against production of ROS, proinflammatory reaction and insulin resistance. Intriguingly, we further find an inverse correlation between FBW7 level and relative higher H_2O_2 level and the severity of obesity-related diabetes. Overall, the results suggest that FBW7 can play a crucial role in modulating inflammatory response through maintaining the intracellular redox homeostasis during HFD insults.

1. Introduction

Obesity is a major risk of metabolic syndrome and type 2 diabetes mellitus (T2DM) and is characterized by increased accumulation of macrophages, neutrophils, and lymphocytes into metabolic organs, such as skeletal muscles, adipose tissues and liver [1,2]. Several lines of evidence now support macrophages as the key cell type that mediate the metabolic tissue inflammation [3,4]. These chronic accumulating macrophages express inflammatory markers, secret proinflammatory cytokines like interleukin 6 (IL-6), interleukin 1β (IL-1β) and tumor necrosis factor-α (TNFα), inhibit insulin signaling in target organs, impair glucose tolerance and insulin insensitivity, and eventually cause T2DM [5,6]. Therefore, targeting this chronic inflammatory aspect of macrophage biology is a therapeutic strategy to improve obesity-related insulin resistance and metabolic syndrome.

FBW7 (F-box and WD repeat domain-containing 7) is a member of the WD40-repeat-containing F-box protein family, and a component of SCF (complex of F-box protein, CUL1 and SKP1)-type ubiquitin ligase, which can recognize, bind and polyubiquitinate the substrates for following degradation by proteasome [7,8]. *FBW7* gene is located on chromosome 4q32, and alternatively spliced into α (nucleus), β (cytoplasmic), and γ (enriched in the nucleolus) isoform. The SCF^{FBW7} complex promotes the ubiquitination and subsequent degradation of numerous proteins such as c-Jun, c-Myc, fetuin-A, Notch, KLF2 and cyclin E [9–14]. Besides its role as a master suppressor, FBW7 has been identified to function in lipid metabolism, viral immunity, cell proliferation, stemness and differentiation [15,16]. Kuppusamy et al. reported that FBW7 controlled the pro-inflammatory signaling by suppression of C/EBPδ expression for proteasomal degradation [17]. In addition, during adipocyte differentiation, decreased expression of FBW7 resulted in the accumulation of proadipogenic proteins such as C/EBPα [18]. However, whether and how FBW7 functions in overnutrition-induced

* Corresponding author. Clinic Center of Human Gene Research, Union Hospital, Tongji Medical College, Huazhong University of Science and Technology, 1277 Jiefang Ave., Wuhan, 430000, China.
E-mail address: cwangunion@hust.edu.cn (C. Wang).
[1] These authors contributed equally to this work.

https://doi.org/10.1016/j.redox.2020.101688
Received 25 May 2020; Received in revised form 10 August 2020; Accepted 13 August 2020
Available online 15 August 2020

inflammation and insulin resistance is poorly understood.

Overnutrition-related insulin resistance is characterized as a state of low-grade chronic inflammation with lipid and glucose alterations mediated partly by activation of adipose tissue macrophages (ATMs) [19,20]. Pathophysiological ROS in ATMs, such as hydroxyl radical (OH•), hydrogen peroxide (H_2O_2) and superoxide anion ($O2\cdot-$), are a key player to contribute to metabolic and physiologic processes [21]. With respect to the development of T2DM, persistent obesity produced more ROS in macrophages, which damage protein, DNA, and cell membranes structures, as well as modulating transcriptional factors activity, leading to chronic inflammation and cell apoptosis [22,23]. Many studies using human and murine macrophages have showed that classically pro-inflammatory macrophages are dependent on disruption of oxidant/antioxidant balance [24,25]. Pyruvate kinase M2 (PKM2), catalyzing the rate-limiting reaction in the glycolytic pathway, plays a crucial role in the glycolytic switch occurring in activated macrophages [26]. PKM2 inhibition is demonstrated to shunt glucose catabolism to the PPP which protect against redox stress by oxidizing glucose 6-phosphate to ribose 5-phosphate and generating NADPH, thus regenerating glutathione (GSH) from glutathione disulfide (GSSG) to modulate hydrogen peroxide to water [27,28]. However, the precise mechanism how to regulate the inflammation driven by PKM2-dependent redox dysfunction has not been fully elucidated and is of central importance to understand the pathogenesis of inflammatory-related diseases.

In this study, we identify PKM2 as a novel target of FBW7 for ubiquitination and degradation. Disruption of FBW7-mediated PKM2 degradation in macrophages markedly alters redox homeostasis, in particular acerbating the obesity-related insulin resistance. This work uncovers a critical module of the redox regulatory network in macrophages and suggests that control of PKM2 stability by FBW7 is a potent mechanism that contributes to the balance of whole body pro-inflammatory and anti-inflammatory status.

2. Materials and methods

2.1. Animal experiments

FBW7$^{fl/fl}$ mice (B6; 129-FBW7tm1Ygu/J) were obtained from The Jackson Laboratory. The mice were crossed with C57BL/6 mice for nine generations before being bred with heterozygous *FBW7*$^{fl/+}$ mice to get the *FBW7*$^{fl/fl}$ mice. *FBW7*$^{fl/fl}$ mice were then crossbred with Lysozyme 2-Cre mice (B6.129P2-Lyz2tm1(cre)Ifo/J; The Jackson Laboratory) to generate myeloid FBW7 deficiency mice. All experimental procedures were approved by the Institutional Animal Care and Use Committee. Male myeloid FBW7 deficiency mice (*FBW7*$^{fl/fl}$*Lysm*$^{Cre+/-}$) aged 7-8-week-old and their control littermates (*FBW7*$^{fl/fl}$*Lysm*$^{Cre-/-}$) were fed a chow diet (CD) or a 60% high fat diet (HFD) (Research Diets, New Brunswick) for 16 weeks. Body weight was measured every two weeks. Following an overnight fast, fasting blood samples for glucose determination were collected from the tail vein and tested by TrueTest glucometer. The intraperitoneal insulin tolerance test (ITT) (0.5 U/kg of body weight) and glucose tolerance test (GTT) (1 g/kg of body weight) were performed after respective 4 h or 12 h of fasting. Blood glucose from the mouse tail vein was measured by TrueTest glucometer every 15–30 min following injection. Insulin concentration was measured with a kit purchased from Crystal Chem. For Shikonin treatment, HFD-fed *FBW7*$^{fl/fl}$*Lysm*$^{Cre+/-}$ or *FBW7*$^{fl/fl}$*Lysm*$^{Cre+/-}$ mice received a daily intraperitoneal injection of vehicle or 2 mg/kg/day Shikonin during the duration of the experiment.

2.2. Acute tissue insulin signaling tests

Overnight-fasted male *FBW7*$^{fl/fl}$*Lysm*$^{Cre-/-}$ and *FBW7*$^{fl/fl}$*Lysm*$^{Cre+/-}$ mice after HFD for 16 weeks were anesthetized with the muscular injection of ketamine/xylazine, followed by portal vein injection of human insulin (0.5 U/kg body weight) or vehicle saline. Five minutes later, the liver, soleus muscle and epididymal fat pads were collected for the determination of phosphorylation of AKT (Thr308) and total AKT by western blotting.

2.3. Biochemical analysis

Plasma levels of mouse IL-6 (431304, BioLegend), IL-1β (MLB00C, R&D Systems) or TNFα (430904, BioLegend) were measured by using ELISA kits. Total triglycerides and cholesterol were measured by Infinity™ Triglycerides Liquid Stable Reagent (Thermo) and Infinity™ Cholesterol Liquid Stable Reagent respectively.

2.4. Western blot analysis

Western blot analysis was measured as described previously [29,30]. Tissue and cell extracts were separated by SDS-PAGE and transferred to nitrocellulose membranes. Blots were probed with the appropriate primary antibodies against PKM2 (Cell signaling technology, 4053), pAKT (Cell signaling technology, 13038), total AKT (Cell signaling technology, 9272), pSTAT3 (Cell signaling technology, 9145), total STAT3 (Cell signaling technology, 9139), NOX4 (Novus, NB110-58849), SOD2 (Cell signaling technology, 13141), NOX2 (Abcam, ab129068), catalase (Cell signaling technology, 14097), 3-nitrotyrosine (Abcam, ab61392), CDK5 (Cell signaling technology, 12134), GSKβ (Cell signaling technology, 12456), FBW7 (BETHYL, A301-721A), Myc (Cell signaling technology, 2276), Flag (Cell signaling technology, 14793), HA (Cell signaling technology, 3724), and β-Actin (Santa Cruz, sc-47778) at 4 °C overnight. The membrane was extensively washed and then incubated with appropriate secondary antibody. Proteins were visualized by using an available chemiluminescence kit (GE Healthcare).

2.5. RNA isolation and quantitative real-time PCR (qPCR)

Total RNA was extracted by using TRIzol reagent (Invitrogen). Reverse transcription was performed using iScript cDNA Synthesis Kit (Bio-Rad). PCR amplification was performed using the SYBR PCR mix (Bio-Rad). The relative RNA amount was normalized with GAPDH or 18S RNA.

2.6. Pyruvate kinase activity assay

Peritoneal macrophages were seeded in 6-well plates (7×10^5 cells/well) and then treated with vehicle or stearic acid (100 μM, 12 h). Pyruvate kinase activity was determined by a commercial kit (Abcam, ab83432).

2.7. Plasmids construction

The coding regions for human FBW7, ΔF-box-FBW7, PKM2, CDK5, and P35 were amplified by PCR and subcloned into the mammalian expression plasmids p3 × FLAG-CMV9, pcDNA3.1-Myc and pcDNA3.1-HA. All constructs were verified by sequencing. The PKM2(S37A) and CDK5 (D145N) was generated by using a QuikChange II site-directed mutagenesis Kit (Stratagene).

2.8. Immunohistochemistry and immunofluorescence staining

Immunohistochemistry staining and Immunofluorescence staining were tested as previously reported [29,31], with antibodies specific against CD68 (Abcam, ab6640 or Bio-Rad, MCA1957) and PKM2 (Cell signaling technology, 4053). The nucleuses were stained with DAPI. Slides were visualized using an OLYMPUS BX53 microscope or ZEISS LSM 800 confocal microscope.

2.9. Cell culture

Peripheral blood mononuclear cells (PBMCs) were isolated by using density gradient centrifugation using Lymphoprep (STEMCELL Technologies). Primary bone marrow-derived macrophages (BMDMs) were collected by flushing the tibia and femur of mice. Cells were cultured with complete Dulbecco's Modified Eagle's Medium (DMEM) medium supplemented with mouse macrophage colony-stimulating factor (M-CSF) recombinant protein for 7 days. Peritoneal macrophages (PMs) were prepared by peritoneal lavage with 10 ml phosphate-buffered saline (PBS) with 10% fetal bovine serum (FBS). After incubation for 3 h at 37 °C, the non-adherent cells were washed away, and adherent cells were collected for experiments. RAW264.7 cells and HEK293T cells were cultured as recommended by American Type Culture Collection (Rockville, MD). For stearic acid treatment, macrophages were treated with stearic acid at a final concentration of 100 μM. The concentration of MG132 (474790, Millipore) treatment is 20 μM. Analysis of protein stability were performed by the Cycloheximide (CHX; 40 mg/ml). We used NAC at a concentration of 5 mM as a ROS scavenger.

2.10. Isolation of stromal vascular fractions and adipose tissue macrophage (ATM)

Epididymal fat pads were excised and centrifuged to remove free leukocytes and erythrocytes. Collagenase D (Roche) was added to 1 mg/ml and incubated at 37 °C for 30 min with shaking. The cell suspension was filtered through a 100-μm filter and centrifuged at 500 g for 5 min. Floating adipocytes and SVF pellets were collected, and the SVFs were resuspended in red-blood-cell lysis buffer (eBioscience) before further analysis. To isolate ATMs, SVFs were washed with PBS and subjected to magnetic immunoaffinity isolation with anti-F4/80 antibodies (MACS; Miltenyi Biotec).

2.11. Two-dimensional gel electrophoresis and LC-MS/MS analysis

Cell lysates from primary macrophages were labeled by Cy3 or Cy5. Cy5-or Cy3-labeled protein was mixed with 2D-DIGE buffer (20 mM dithiothreitol, 4% CHAPS, 7 M urea, 2 M thiourea,0.5% IPG buffer). Isoelectric focusing (IEF) was performed on 24-cm IPG strips, pH 4.0–7.0. The second-dimension electrophoresis was performed under 10% SDS-polyacrylamide gels. The 2D gels were then scanned on a Typhoon 9410 imager (GE Healthcare Life Sciences). Protein spots displaying an average $\geq$ 1.5-fold change ($P < 0.05$) in abundance between WT or FBW7 KO samples were selected for picking on an Ettan Spot Picker (GE Healthcare Life Sciences). For each treatment, images with 3 biological repeats were applied for the protein abundance analysis. Mass spectra was performed using Mascot search engine for protein identification. Database searching was subjected to the Mascot program.

2.12. Measurement of pentose phosphate pathway intermediates

Peritoneal macrophages were washed and solubilized in ice-cold methanol/water (85/15, v/v). After repeated vortexing for 10 min on dry ice, cell samples were centrifuged (13000 rpm, 4 °C, 10 min). Isotope labeled internal standards were added and then evaporated in a vacuum concentrator plus (Eppendorf) at 30 °C. After evaporation, each tube was resolved in 50 μL water methanol/water (50/50, v/v) for PPP metabolites and subsequently transferred to the LC-MS system.100% 10 mmol/L ammonium acetate (pH 9.0) as mobile phase A and 100% acetonitrile as mobile phase B. Mass spectrometry was performed with electrospray ionization in negative mode by using a QTrap 5500 mass spectrometer (Sciex). Data acquisition were managed through the software Analyst 1.6.2. Area under the peak was used for quantification of the metabolites and the specific MRM transitions were normalized to the protein content of the peritoneal macrophages and to appropriated isotope labeled internal standards.

2.13. Determination of GSH/GSSG and NADPH/NADP $^+$ ratios

Fresh cells were used immediately to determine the GSH/GSSG (ab138881, Abcam) and NADPH/NADP $^+$ ratios (ab176724, Abcam) using commercially available kits. Protein concentrations of the cells lysates or actual tissue weight were used for normalization.

2.14. H_2O_2 measurement

Reagent preparation and all steps of the procedure were performed in the dark and all reagents were prepared immediately before use. Fresh cells were incubated in Hepes-Tyrode solution containing 50 μmol/L Amplex Red reagent (Invitrogen), with or without 0.2 U/ml horseradish peroxidase (Invitrogen). The developed fluorescence in each sample was measured at Ex/Em 530/590. Relative fluorescence units from the samples without horseradish peroxidase (background) were subtracted from the corresponding samples with horseradish peroxidase. Finally, all values were normalized to wild-type.

2.15. Glycolysis assays

Cellular extracellular acidification rate (ECAR) were measured in peritoneal macrophages. Measurements were taken using a Seahorse Bioscience XF96 extracellular analyzer. Three measurements were taken before and after addition of glucose (10 mM), oligomycin (1 μM), and 2-DG (50 mM). ECAR were calculated by the Seahorse Wave software.

2.16. Immunoprecipitation

Briefly, 500 μg of protein extracts were incubated with the indicated antibodies at 4 °C overnight, and protein-A/G agarose was added for another 3 h. The immunoprecipitates were pelleted by centrifugation and washed with RIPA lysis buffer. The pellets were suspended in SDS loading buffer and subjected to immunoblot assays.

2.17. Analysis of human samples

All procedures involving human samples complied with the principles outlined in the Declaration of Helsinki. All of the selected patients provided written, informed consent. The experiment was supported by the Ethics Committee of Tongji Medical College of Huazhong University of Science and Technology. Human blood samples were classified as obese or lean based on BMI following World Health Organization criteria: control (n = 33, BMI 22.67 ± 1.90); obesity (n = 82, BMI 31.89 ± 1.22). Obese were classified as with or without diabetes based on fasting blood glucose following the American Diabetes Association (ADA) criteria:obesity without diabetes (fasting plasma glucose (FPG) level 6.2 ± 0.7 mmol/L); obesity with diabetes (fasting plasma glucose (FPG) level 11.6 ± 1.9 mmol/L).

2.18. Statistical analysis

GraphPad Prism software was used to assess statistical significance. Results are presented as mean ± SEM. Statistical differences were evaluated by unpaired two-tailed Student's t-test for two groups comparation, while differences between three groups or more were compared by one-way ANOVA followed by Bonferroni posttest. The statistical significance of correlations was analyzed by Pearson's correlation coefficient analysis. Significance was set at $P < 0.05$.

3. Results

3.1. Myeloid FBW7 deficiency exacerbates insulin resistance in HFD-fed mice

To explore whether FBW7 deficiency in macrophages exerts

metabolic disorders, we intercrossed floxed FBW7 mice with the Lysozyme 2-Cre (Lysm-Cre) line to create myeloid-specific FBW7-knockout mice, in which protein level of FBW7 was abrogated in BMDMs and PMs (Fig. S1A). In comparison to their *FBW7*$^{fl/fl}$*Lysm*$^{Cre-/-}$ counterparts, *FBW7*$^{fl/fl}$*Lysm*$^{Cre+/-}$ mice showed no defective developmental phenotypes and had insignificant differences in body weight after CD feeding (Fig. S1B). Next, we compared glucose tolerance and insulin response to explore their glucose homeostasis. As shown in Supplementary Fig. 1D and E, FBW7 deficiency mildly disrupted the glucose profile in the IP-GTT and IP-ITT. To enlarge the effect, mice were administrated by HFD for 16 weeks to generate obesity. The results exhibited that there was no statistic difference in body and tissue weight between HFD-fed *FBW7*$^{fl/fl}$ *Lysm*$^{Cre-/-}$ and *FBW7*$^{fl/fl}$ *Lysm*$^{Cre+/-}$ mice (Figs. S1B and C). Interestingly, HFD-fed *FBW7*$^{fl/fl}$ *Lysm*$^{Cre+/-}$ mice showed higher glucose level and hyperinsulinemia, and severely disrupted insulin sensitivity as evident by GTT and ITT (Fig. 1A–D), while did not alter hypercholesterolemia and hypertriglyceridemia (Figs. S1F and G). We then analyzed the insulin signaling in soleus muscle, liver and epididymal fat respectively in mice on HFD. AKT (Thr308) phosphorylation stimulated by insulin was significantly attenuated in *FBW7*$^{fl/fl}$*Lysm*$^{Cre+/-}$ mice relative to controls (Fig. 1E). These data demonstrate that myeloid FBW7 deficiency could exacerbate insulin resistance in HFD-induced obesity.

3.2. Myeloid FBW7 deficiency aggravates HFD-induced oxidative stress and inflammation

Obesity promotes macrophages infiltration in metabolic tissue and the induction of a pro-inflammatory state and insulin resistance [32]. The potential plasma and tissue levels of proinflammatory cytokines in *FBW7*$^{fl/fl}$*Lysm*$^{Cre-/-}$ and *FBW7*$^{fl/fl}$*Lysm*$^{Cre+/-}$ mice were then investigated. Upon chow diet feeding, *FBW7*$^{fl/fl}$*Lysm*$^{Cre+/-}$ mice displayed no significant differences with respect to serum TNFα, IL-6, and IL-1β level in comparison with *FBW7*$^{fl/fl}$*Lysm*$^{Cre-/-}$ mice (Fig. 2A). However, when we detected the gene expression profiles of epiWAT, subWAT and liver by RT-qPCR, some inflammatory related genes (TNFα, IL-1β, iNOS) expression were mildly increased (Fig. S1H). Interestingly, under 16-week HFD treatments, the plasma contents of IL-1β, TNFα and IL-6 were obviously higher in *FBW7*$^{fl/fl}$*Lysm*$^{Cre+/-}$ mice than *FBW7*$^{fl/fl}$*Lysm*$^{Cre-/-}$ mice (Fig. 2A). We also measured the proinflammatory gene expression profiles of epiWAT and liver by RT-qPCR. The results showed that upon HFD feeding, expression of genes encoding molecules typically linked to the progression of insulin resistance (e.g. TNFα, iNOS, IL-1β, and IL-6) (Fig. 2B) were increased in *FBW7*$^{fl/fl}$*Lysm*$^{Cre+/-}$ mice. In addition, immunohistochemical (IHC) analysis revealed that the number of infiltrating CD68^{+} macrophages was significantly upregulated in epiWAT of HFD-fed *FBW7*$^{fl/fl}$*Lysm*$^{Cre+/-}$ mice (Fig. 2C), these findings indicate in response to HFD myeloid FBW7 deficiency sharpens systemic inflammation in mice.

It has been reported that increased reactive oxygen in macrophages may lead to chronic inflammation and hyperglycemia [33]. We isolated F4/80-positive adipose tissue macrophages (ATMs) from HFD-fed *FBW7*$^{fl/fl}$*Lysm*$^{Cre-/-}$ and *FBW7*$^{fl/fl}$*Lysm*$^{Cre+/-}$ mice. The results from 3-nitrotyrosine footprint showed a significant increase in oxidative stress in ATMs from *FBW7*$^{fl/fl}$*Lysm*$^{Cre+/-}$ mice (Fig. 2D). Consistently, the increased H_2O_2 levels induced by HFD was also significant upregulated (Fig. 2E). Inversely, the ratios of GSH/GSSG and NADPH/NADP^{+} were relatively lower in ATMs from *FBW7*$^{fl/fl}$*Lysm*$^{Cre+/-}$ mice than that from *FBW7*$^{fl/fl}$*Lysm*$^{Cre-/-}$ mice (Fig. 2F and G). These findings suggest that myeloid FBW7 deficiency up-regulates oxidative stress and proinflammatory reaction after HFD treatment.

3.3. FBW7 negatively regulates levels of PKM2

To search for the potential factors that might be regulated by FBW7 in macrophages, we isolated peritoneal macrophages from WT (*FBW7*$^{fl/fl}$*Lysm*$^{Cre-/-}$) and FBW7 deficiency (*FBW7*$^{fl/fl}$*Lysm*$^{Cre+/-}$) mice, and performed the two-dimensional gel electrophoresis which used different labeling for WT and FBW7 deficiency protein samples. A number of differential proteins were identified and analyzed by Mass spectrometry (Fig. 3A). As depicted in Fig. 3B, FBW7 deficiency dramatically influenced the metabolic pathway in macrophages by KEGG pathway analysis. Among them, PKM2 scored the highest on the peptide hit list. Then protein extracts of peritoneal macrophages and stromal-vascular cell fraction of adipose tissues from WT and FBW7 deficiency mice were applied to Western blot assay. PKM2 expression was efficiently upregulated by FBW7 deletion (Fig. 3C and Fig. S2). Parallel to the western blotting results, confocal microscopy showed an abundant protein level of PKM2 due to FBW7 deficiency (Fig. 3D). These results suggest that expression of PKM2 could be highly regulated by FBW7 in macrophages.

3.4. FBW7 mediates the ubiquitination and degradation of PKM2

To further explore whether FBW7 regulated PKM2 protein stability,

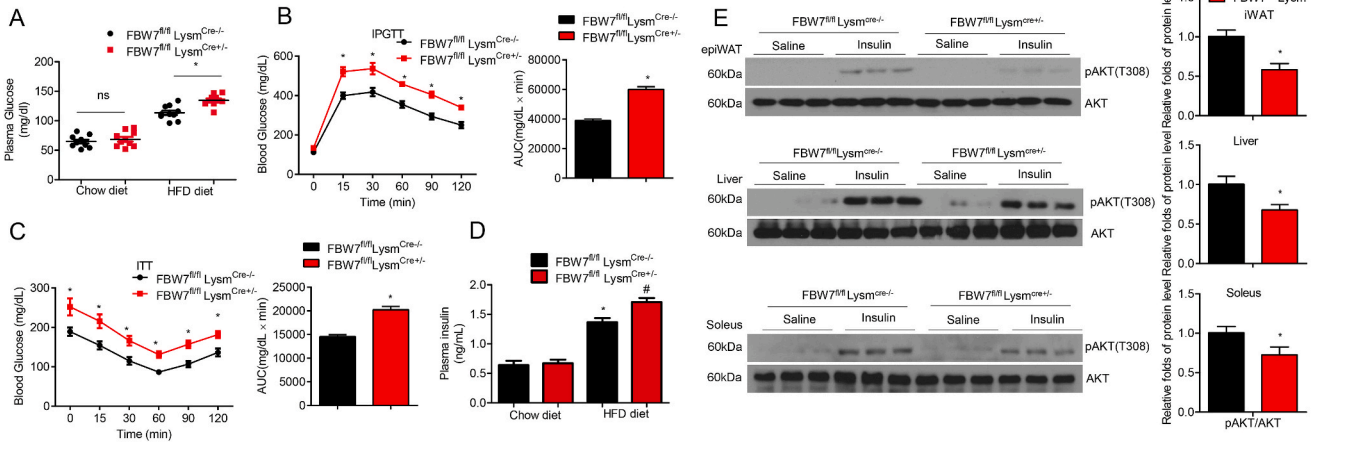

Fig. 1. FBW7 deficiency in myeloid cells exacerbates insulin resistance in obesity.
Age-matched *FBW7*$^{fl/fl}$*Lysm*$^{Cre-/-}$ and *FBW7*$^{fl/fl}$*Lysm*$^{Cre+/-}$ mice were fed with CD or HFD for 16 weeks (n = 15). Mice were fasted, and plasma glucose (**A**), GTT (**B**), ITT (**C**), and plasma insulin (**D**) were tested respectively. (**E**) Acute insulin signaling in liver, soleus, and epididymal fat (epiWAT) were detected by immunoblot analysis with the indicated antibodies. Statistical significance was performed using two-tailed t-tests for two groups and using ANOVA for multiple comparison. *$P <$ 0.05 vs *FBW7*$^{fl/fl}$*Lysm*$^{Cre-/-}$. $^{\#}P < 0.05$ vs *FBW7*$^{fl/fl}$*Lysm*$^{Cre-/-}$ + HFD. All values are means ± SEM.

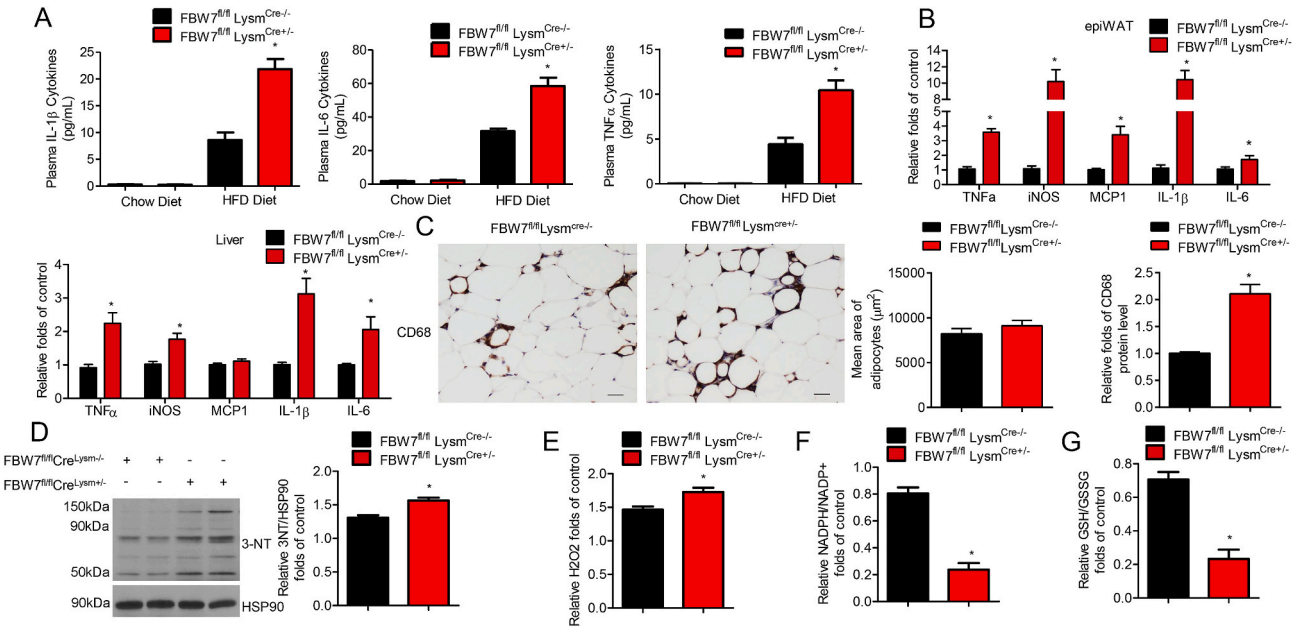

Fig. 2. FBW7 deficiency in myeloid cells exacerbates redox stress and inflammation in obesity.
Age-matched *FBW7*$^{fl/fl}$*Lysm*$^{Cre-/-}$ and *FBW7*$^{fl/fl}$*Lysm*$^{Cre+/-}$ mice were fed with CD or HFD for 16 weeks (n = 15). (**A**) Plasma concentrations of cytokines (TNFα, IL-1β and IL-6) were tested. (**B**) The relative mRNA levels of inflammatory cytokine (TNFα, IL-1β, iNOS, IL-6 and MCP1) in epididymal fat (epiWAT) and liver. (**C**) Representative images of CD68 immunohistochemistry in epiWAT sections. Scale bars, 50 μm. (**D**) 3-Nitrotyrosine (3-NT) levels in ATMs from *FBW7*$^{fl/fl}$*Lysm*$^{Cre-/-}$ and *FBW7*$^{fl/fl}$ *Lysm*$^{Cre+/-}$ mice. (**E**) H_2O_2 levels in in ATMs from *FBW7*$^{fl/fl}$*Lysm*$^{Cre-/-}$ and *FBW7*$^{fl/fl}$ *Lysm*$^{Cre+/-}$ mice. (**F** and **G**) GSH/GSSG and NADPH/$NADP^+$ ratios in ATMs from *FBW7*$^{fl/fl}$*Lysm*$^{Cre-/-}$ and *FBW7*$^{fl/fl}$ *Lysm*$^{Cre+/-}$ mice. Statistical significance was performed using two-tailed t-tests for two groups and using ANOVA for multiple comparison. **P* < 0.05 vs *FBW7*$^{fl/fl}$*Lysm*$^{Cre-/-}$. All values are means ± SEM.

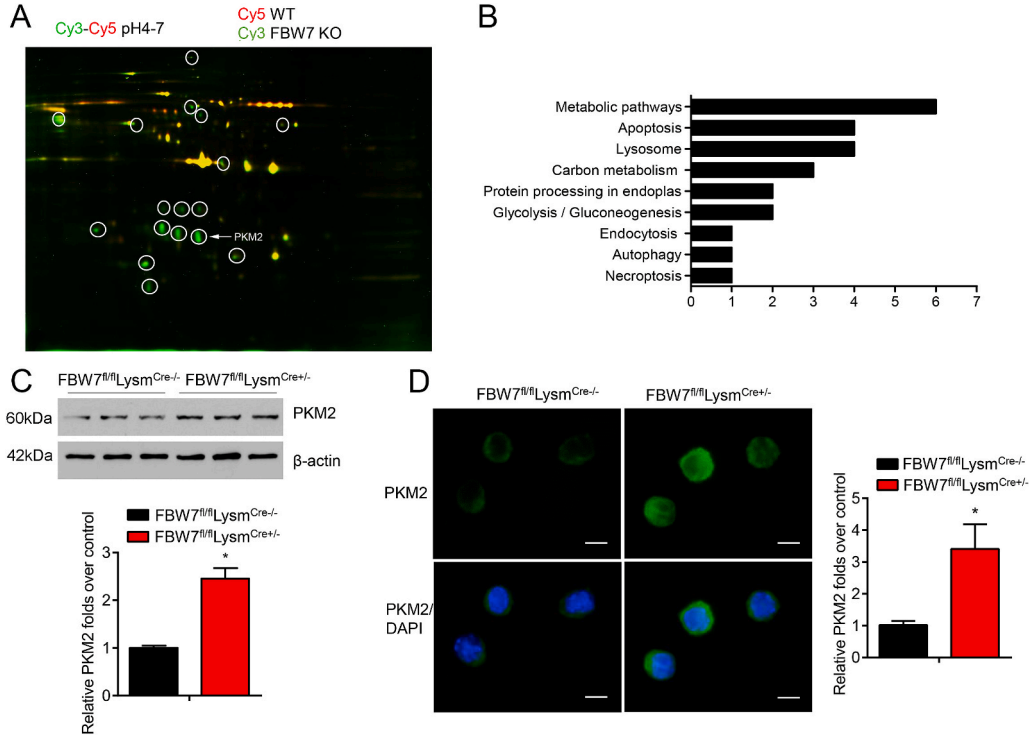

Fig. 3. FBW7 negatively regulates the level of PKM2.
(**A**) Total proteins from peritoneal macrophages of *FBW7*$^{fl/fl}$*Lysm*$^{Cre-/-}$ and *FBW7*$^{fl/fl}$*Lysm*$^{Cre+/-}$ mice were separated electrophoretically by 2D gel electrophoresis, then differential spots were cut and subjected to mass spectrometry analysis (n = 3). *FBW7*$^{fl/fl}$*Lysm*$^{Cre-/-}$ (WT) was labeled by Cy5, *FBW7*$^{fl/fl}$*Lysm*$^{Cre+/-}$ (FBW7 KO) was labeled by Cy3. (**B**) The identified differential proteins were applied to KEGG pathways analysis. The metabolic pathway scored the highest on the pathway analysis list. (**C**) Immunoblot analysis of PKM2 expression in *FBW7*$^{fl/fl}$*Lysm*$^{Cre-/-}$ and *FBW7*$^{fl/fl}$*Lysm*$^{Cre+/-}$ peritoneal macrophages (n = 5). (**D**) Representative immunofluorescent staining of PKM2 in *FBW7*$^{fl/fl}$*Lysm*$^{Cre-/-}$ or *FBW7*$^{fl/fl}$*Lysm*$^{Cre+/-}$ ATMs. Nuclei were stained with DAPI (n = 5). Scale bars, 10 μm. Statistical significance was performed using two-tailed t-tests for two groups and using ANOVA for multiple comparison. **P* < 0.05 vs *FBW7*$^{fl/fl}$*Lysm*$^{Cre-/-}$. All values are means ± SEM.

shRNA-mediated silencing of FBW7 in Raw264.7 cells was able to upregulate the protein level of endogenous PKM2, which was due to an increase in the half-life of endogenous PKM2 (Fig. 4A). Next, we wondered whether FBW7 led to PKM2 downregulation via proteasome degradation. Raw264.7 cells, co-transfected with Myc-FBW7 and Flag-PKM2, were incubated with DMSO or MG132, a potent 26S proteasome inhibitor. MG132 stimulation significantly blocked the down-regulation of PKM2 expression under FBW7 supplement (Fig. 4B). Furthermore, we also detected the mRNA level of PKM2, which showed that FBW7 deficiency had no effects on the transcriptional level of PKM2 (Fig. 4C), all suggesting that FBW7 targets PKM2 for proteasomal degradation. Moreover, three splice-variant isoforms (α, β and γ) of

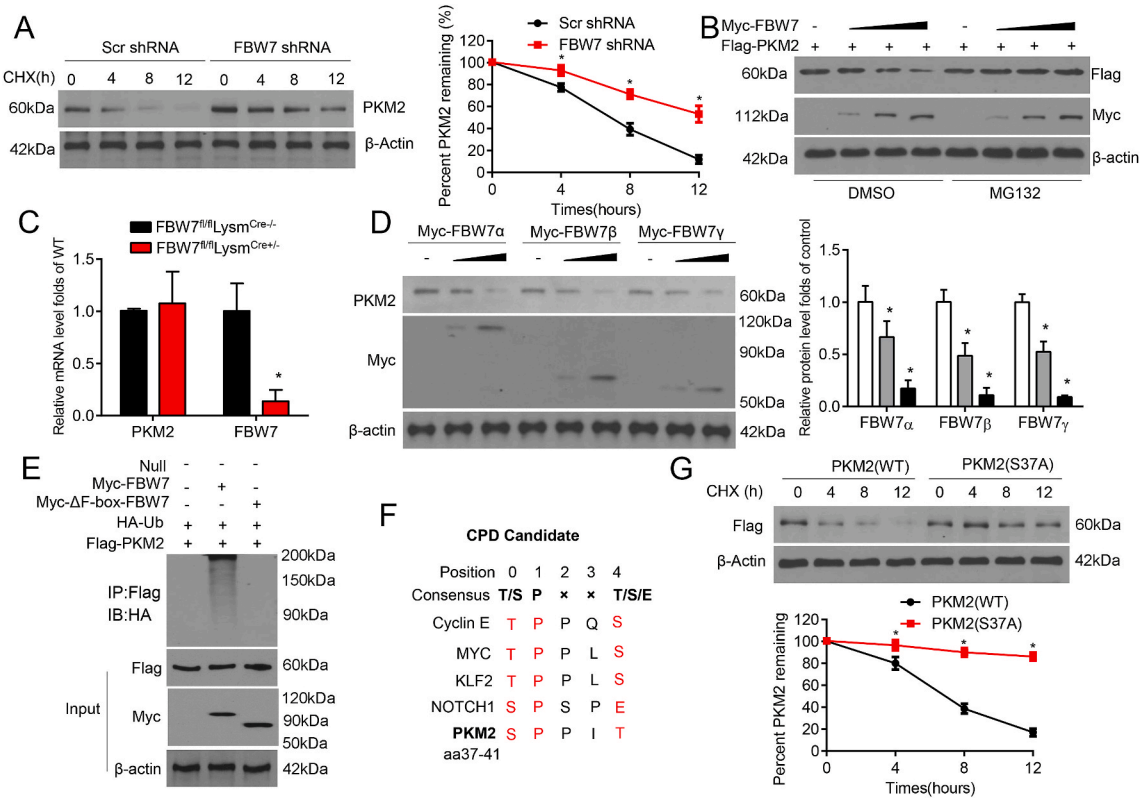

Fig. 4. FBW7 mediates the ubiquitination and degradation of PKM2.
(**A**) Raw264.7 cells, pre-transfected with Scr shRNA and FBW7 shRNA, were treated with CHX (40 mg/ml) for indicated hours. Cell lysates were subjected to Western blot analysis (n = 5). (**B**) Flag-PKM2 was co-expressed with empty vector or different contents of Myc-FBW7 plasmids in Raw264.7 cells. PKM2 and FBW7 protein levels were tested by using western blotting (n = 5). (**C**) Real-time qPCR assay analysis of PKM2 in $FBW7^{fl/fl}Lysm^{Cre-/-}$ and $FBW7^{fl/fl}Lysm^{Cre+/-}$ peritoneal macrophages (n = 5). (**D**) The protein level of PKM2 under different FBW7 isoforms was detected by western blotting (n = 5). (**E**) HEK293T cells were transfected with Myc-FBW7 or Myc-ΔF-box-FBW7 along with vectors for HA-Ub and Flag-PKM2, and then treated with MG132. Protein lysates were subject to immunoprecipitation with Flag antibody and Western blot with HA antibody (n = 5). (**F**) Sequence alignment of PKM2 with the phospho-degron sequences recognized by FBW7. (**G**) HEK293T cells transfected with Myc-FBW7 along with Flag-PKM2 (WT) or Flag-PKM2 (S37A) and treated with CHX (40 mg/ml) for indicated hours. Cell lysates were subjected to Western blot assay to detect PKM2 level (n = 5). Statistical significance was assessed using two-tailed t-tests for two groups and using ANOVA for multiple comparison. *$P < 0.05$ vs Scr shRNA, Flag-PKM2 (WT) or $FBW7^{fl/fl}Lysm^{Cre-/-}$. All values are means ± SEM.

FBW7 have been identified. Despite their different subcellular localization, our results demonstrated that forced expression of FBW7α, β, and γ could all result in the decreased expression of endogenous PKM2 protein in Raw264.7 cells (Fig. 4D).

Since FBW7 is an E3 ubiquitin ligase, its function is driven by its association and ubiquitination with other factors. It was possible that PKM2 might be as a ubiquitin substrate of FBW7. As depicted in Fig. 3E, we found that PKM2 was polyubiquitinated by wild-type FBW7α, but not the enzymatically dead mutant (ΔF-box-FBW7) [34] (Fig. 4E). These results suggest that FBW7 mediates PKM2 ubiquitination and negatively suppresses its expression. Phosphorylated Ser/Thr residues in the CPD motif are recognized by FBW7, and PKM2 harbored one perfectly matched (S37) FBW7-binding motif after screening (Fig. 4F). It is rational that the amino acid of Ser37 might be required for ubiquitination of PKM2 through FBW7. We generated one mutant of PKM2 (S37A), and protein stability assays demonstrated that the PKM2-S37A prolonged the half-life of PKM2 protein regardless of FBW7 (Fig. 4G). These data strongly indicate that FBW7 mediates the ubiquitination of PKM2 via Ser37.

3.5. FBW7 diverts glycolysis to combat oxidative stress via PKM2 in macrophages

Considering that PKM2 catalyzes the rate-limiting reaction of the glycolytic pathway, we next analyzed the levels of glycolytic metabolites. In parallel with increased PKM2 levels, FBW7 deletion raised pyruvate kinase activity, and the downstream production of phosphoenolpyruvate (PEP) and lactate in stearic acids-primed peritoneal macrophages (Fig. 5A–C). Consistently, in the ECAR assay, FBW7-deficient macrophages exhibited higher levels of the basal condition and the maximum glycolytic capacity after glucose or oligomycin treatment (Fig. 5D). It is reported that the shift between glucose catabolism and pentose phosphate pathway (PPP) altered the generation of equivalents required for the GSH generation and ROS detoxification(28). FBW7 deficiency in macrophages resulted in a reduce in the majority of PPP intermediates, and cellular NADPH and GSH levels were dramatically lower in FBW7-deleted macrophages than in WT cells (Fig. 5E–H). More interestingly, when we silenced PKM2 via shRNA, the above deleterious effects by FBW7 deficiency on the cellular $NADPH/NADP^+$ and GSH/GSSG ratios were nearly abolished (Fig. 5I and J). ROS derives from some cellular sources, foremost mitochondria and nicotinamide adenine dinucleotide phosphate-oxidases (NOX) [35]. We also measured the expression levels of ROS generating enzymes, such as NOX2 or NOX4, and antioxidative enzymes, such as catalase or SOD2. FBW7 deficiency in macrophages led to an increase in the expression of NOX2 and NOX4, and a suppression in the protein level of SOD2 (Fig. S3). Taken together, FBW7 deficiency, associated with higher PKM2 levels, leads to less PPP flux and followingly more oxidative stress in macrophages.

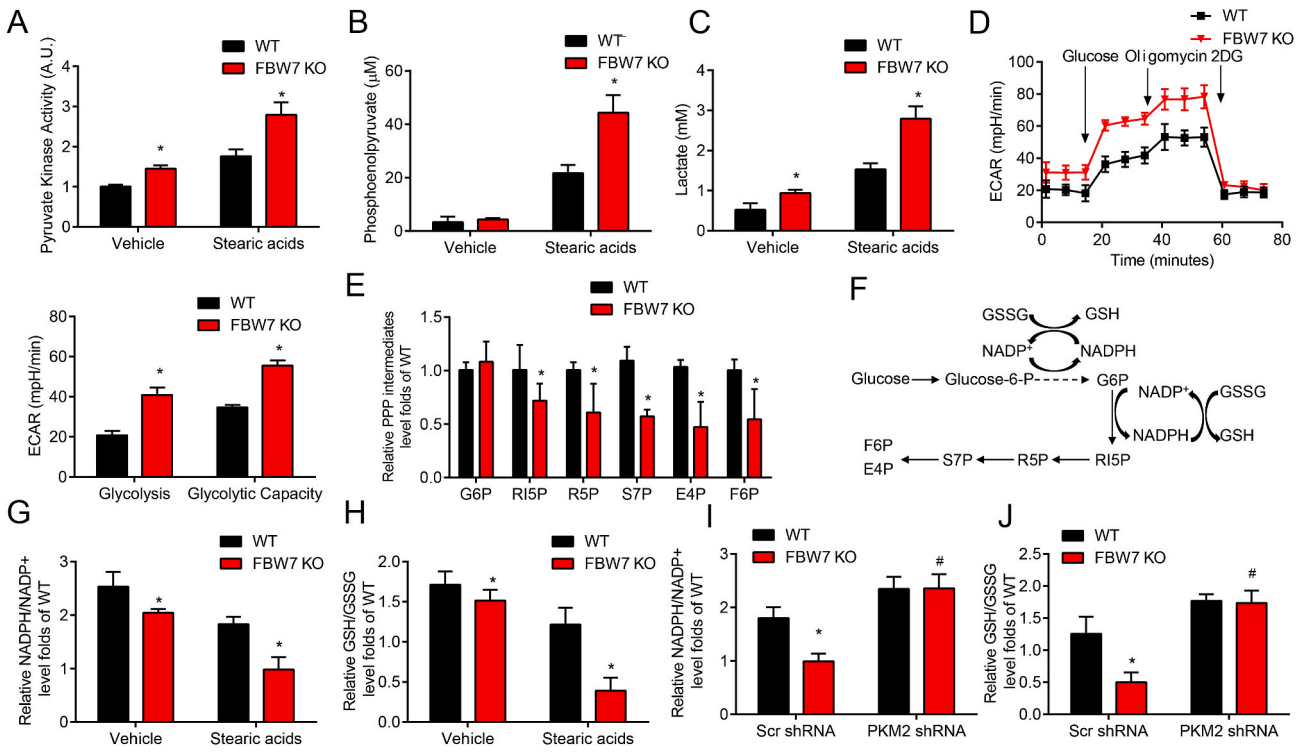

Fig. 5. FBW7 deficiency in macrophages selectively increases oxidative stress via PKM2.
(**A-C**) Peritoneal macrophages from *FBW7*$^{fl/fl}$*Lysm*$^{Cre-/-}$ (WT) and *FBW7*$^{fl/fl}$*Lysm*$^{Cre+/-}$ (FBW7 KO) mice were treated with or without stearic acids (n = 5). Pyruvate kinase activity (**A**), phosphoenolpyruvate (**B**) and lactate (**C**) levels were assayed using the indicated commercial kits. (**D**) Extracellular acidification rate (ECAR) in WT and FBW7-deficiency peritoneal macrophages in response to indicated drugs. (**E**) Quantification of PPP intermediates; fructose-6-P (F6P), erythrose-4-P (E4P), sedoheptulose-7-P (S7P), ribose-5-P (R5P), ribulose-5-P (Rl5P), and gluconate-6-P (G6P) in macrophages from WT and FBW7 KO mice. (**F**) Links among the pentose phosphate pathway, generation of NADPH and GSH. The NADPH/NADP$^+$ (**G**) and GSH/GSSG ratios (**H**) in PMs from WT and FBW7 KO mice were measured under stearic acids treatment (n = 5). (**I** and **J**) Peritoneal macrophages from WT and FBW7 KO mice were transduced by Scr shRNA or PKM2 shRNA, and the NADPH/NADP$^+$ and GSH/GSSG ratios were measured (n = 5). Statistical significance was performed by using ANOVA for multiple comparison. $^*P < 0.05$ vs Scr shRNA or WT, $^{\#}P < 0.05$ vs FBW7 KO + Scr shRNA. All values are means ± SEM.

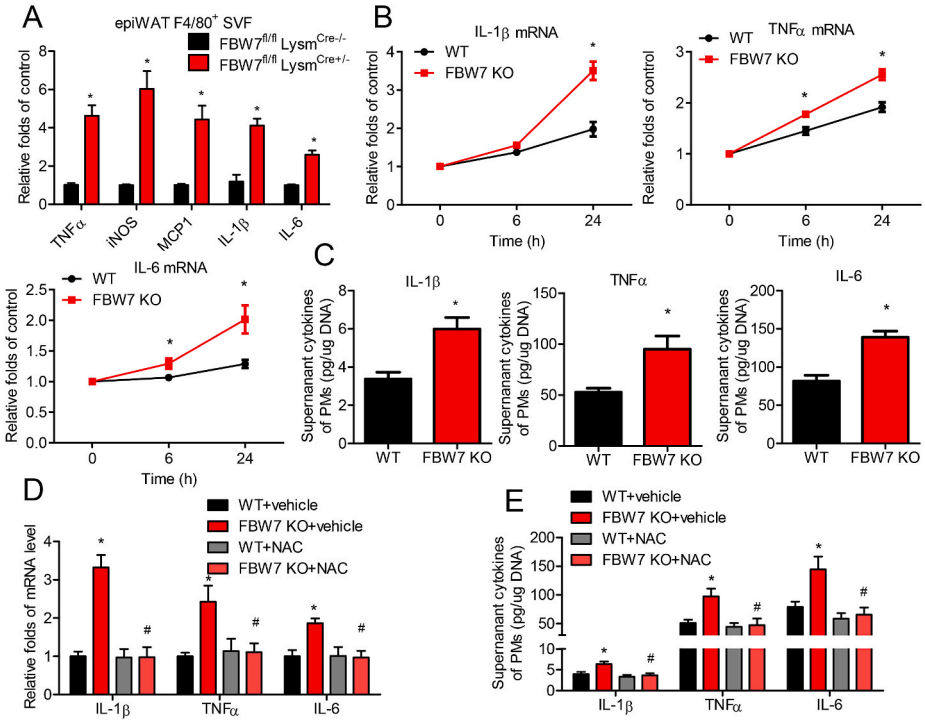

Fig. 6. Oxidative stress mediates the proinflammatory reaction in FBW7 deficiency macrophages.
(**A**) The transcriptional levels of inflammatory cytokine (TNFα, IL-1β, iNOS, IL-6 and MCP1) in epididymal fat-derived macrophages (F4/80$^+$ SVF) (n = 8). (**B**) TNFα, IL-1β and IL-6 mRNA levels in PMs from *FBW7*$^{fl/fl}$*Lysm*$^{Cre-/-}$(WT) and *FBW7*$^{fl/fl}$*Lysm*$^{Cre+/-}$ (FBW7 KO) mice treated with stearic acid (100 μM) (n = 5). (**C**) The contents of cytokines (IL-1β, TNFα and IL-6) in the conditional culture medium of PMs treated with stearic acid for 24 h (n = 5). (**D** and **E**) PMs from WT and FBW7 KO mice were treated with stearic acid in presence or absence of NAC (5 mM). (**D**) TNFα, IL-1β and IL-6 mRNA levels were tested by qPCR (n = 5). (**E**) The contents of cytokines (IL-1β, TNFα and IL-6) in the supernatant were tested by ELISA (n = 5). Statistical significance was assessed using two-tailed t-tests for two groups and using ANOVA for multiple comparison. $^*P < 0.05$ vs WT or *FBW7*$^{fl/fl}$*Lysm*$^{Cre-/-}$; $^{\#}P < 0.05$ vs FBW7 KO + Vehicle. All values are means ± SEM.

3.6. Excessive oxidative stress mediates the proinflammatory reaction in FBW7 deficiency macrophages

We next wondered whether the disruption of redox homeostasis in macrophage contributes to the following inflammation response. To underlie the downstream induction of inflammation in FBW7-deficiency macrophages *in vivo*, we isolated F4/80-positive ATMs from HFD-fed $FBW7^{fl/fl}Lysm^{Cre-/-}$ and $FBW7^{fl/fl}Lysm^{Cre+/-}$ mice. ATMs from $FBW7^{fl/fl}Lysm^{Cre+/-}$ mice displayed a significant upregulation in the mRNA levels of IL-1β, TNFα, iNOS, MCP1 and IL-6 (Fig. 6A). Isolated PMs were primed with steric acids to stimulate pro-inflammatory responses *in vitro*. PMs from $FBW7^{fl/fl}Lysm^{Cre+/-}$ mice showed a significant increase in TNFα, IL-1β and IL-6 mRNA (Fig. 6B). Consistently, these PMs synthesized and secreted more TNFα, IL-1β, and IL-6 protein in the supernatant (Fig. 6C), suggesting FBW7 deficiency accelerates the proinflammatory reaction in macrophages.

In order to verify whether the inflammation response was attributed to oxidative stress in macrophages, Oxidative stress was depleted using an antioxidant N-acetyl-cysteine (NAC). As expected, NAC could significantly reverse the elevated IL-1β, IL-6 and TNFα levels in cells lysates or supernatant from FBW7-deficient macrophages under steric acids treatment (Fig. 6D and E). Thus, oxidative stress mediates the enhanced proinflammatory activation in macrophages under FBW7 deficiency.

3.7. PKM2 is required for oxidative stress, inflammation and insulin resistance in FBW7 deficiency mice

To further confirm the functional role of PKM2 in FBW7 deficiency mice, immunofluorescence staining first showed increased PKM2 expression in WAT from HFD-fed $FBW7^{fl/fl}Lysm^{Cre+/-}$ mice, which was colocalized with macrophage antigen CD68 (Fig. 7A). We next tested whether inhibition of PKM2 by Shikonin [36,37], a potent PKM2 inhibitor in macrophages, could ameliorate abnormal pyruvate kinase activity, glucose metabolism and inflammation in HFD-fed myeloid FBW7 deficiency mice. HFD-fed $FBW7^{fl/fl}Lysm^{Cre-/-}$ or $FBW7^{fl/fl}Lysm^{Cre+/-}$ mice received a daily injection of vehicle or 2 mg/kg/day Shikonin during the duration of the experiment. Compared to $FBW7^{fl/fl}Lysm^{Cre+/-}$ mice receiving vehicle, Shikonin administration abrogated the decreased GSH/GSSG and NADPH/NADP $^{+}$ ratios, and suppressed the pyruvate kinase activity and H_2O_2 level in ATMs (Fig. 7B–D and Fig. S4). More importantly, $FBW7^{fl/fl}Lysm^{Cre+/-}$ mice treated with Shikonin showed an dramatical reduce in the expression of some proinflammatory factors, like TNFα, IL-6, and IL-1β in the serum

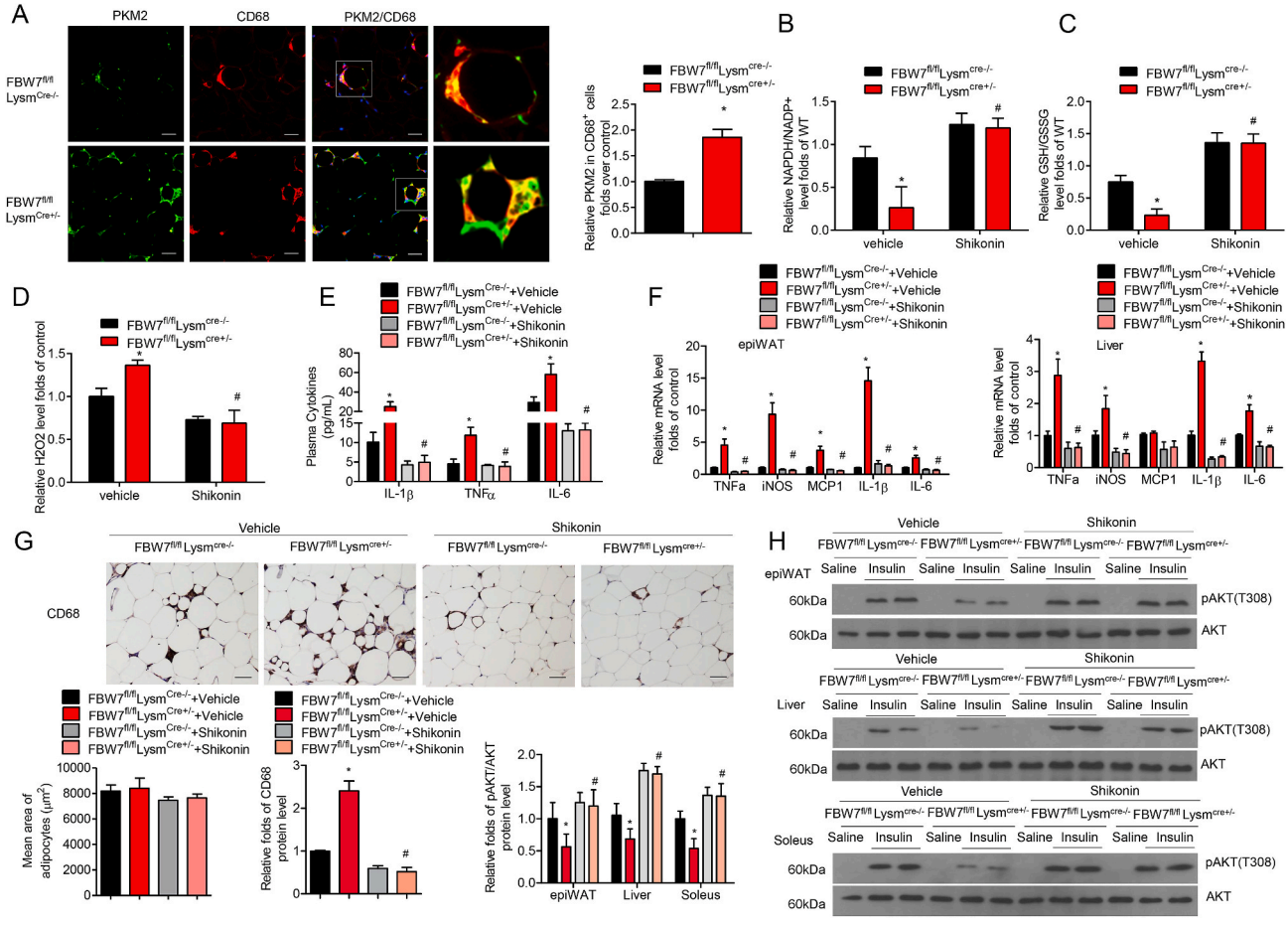

Fig. 7. PKM2 mediates inflammation activation and insulin resistance in FBW7 deficiency mice.
(**A**) Representative immunofluorescence images of PKM2 and CD68 in epWAT sections from $FBW7^{fl/fl}Lysm^{Cre-/-}$ and $FBW7^{fl/fl}Lysm^{Cre+/-}$ mice on HFD for 16 weeks, and the relative quantification (n = 10). Scale bars, 50 μm. (**B**–**H**) HFD-fed $FBW7^{fl/fl}Lysm^{Cre-/-}$ or $FBW7^{fl/fl}Lysm^{Cre+/-}$ mice received a daily injection of vehicle control or 2 mg/kg/day Shikonin during 16 weeks (n = 15). NADPH/NADP $^{+}$ ratio (**B**), GSH/GSSG ratio (**C**) and H2O2 content (**D**) in ATMs were measured. (**E**) Plasma contents of cytokines (TNFα, IL-1β and IL-6) in the mice were tested. (**F**) Relative mRNA levels of inflammatory cytokine (TNFα, IL-1β, iNOS, MCP1 and IL-6) in epididymal fat (epiWAT) and liver of mice. (**G**) Representative images of CD68 immunohistochemistry in epiWAT sections. Scale bars, 50 μm. (**H**) Acute insulin signaling in liver, soleus and epididymal fat (epiWAT) were detected by immunoblot analysis with the indicated antibodies. Statistical significance was performed using two-tailed t-tests for two groups and using ANOVA for multiple comparison. $^{*}P < 0.05$ vs $FBW7^{fl/fl}Lysm^{Cre-/-}$ or $FBW7^{fl/fl}Lysm^{Cre-/-}$ + Vehicle; $^{\#}P < 0.05$ vs $FBW7^{fl/fl}Lysm^{Cre+/-}$ + Vehicle. All values are means ± SEM.

samples (Fig. 7E), consistent with the expression of genes (e.g., TNFα, IL-1β, iNOS, and IL-6) in liver and epiWAT (Fig. 7F). Furthermore, Shikonin treatment led to less CD68-positive macrophages infiltration in WAT (Fig. 7G). In addition, we also analyzed the insulin signaling in mice on HFD. Shikonin treatment significantly improved the phosphorylated AKT(Thr308) level in liver, soleus muscle and epididymal fat, respectively, in relative to vehicle controls (Fig. 7H). All these data suggest that PKM2 is required for ROS production, inflammation activation and insulin resistance in myeloid FBW7 deficiency mice.

3.8. FBW7 inversely correlates with the development of obesity-related diabetes

Since many evidences has established a pivotal role for macrophages in the progression of chronic metabolic diseases, we next explore whether macrophage FBW7 was involved in the obesity-related chronic inflammation process. We divided human samples into three groups based on the different stages of obesity and diabetes. Strikingly, both mRNA and protein levels of FBW7 were decreased in the PBMCs of obese samples compared to the controls (Fig. 8A and B), suggesting relative expression of FBW7 was negatively related with obesity-related diabetes progression and poor outcome of diabetes patients. We also detected the contents of glucose, triglyceride, cholesterol and CRP in human blood samples, and calculated the correlation between the markers and the mRNA level of FBW7. As depicted in Fig. 8C and D, a negative association between relative FBW7 expression and blood glucose or serum CRP levels, but not triglyceride or cholesterol (Fig. S5), were observed, suggesting that FBW7 was strongly negative with the severity of glucose and CRP level in obesity. Next, we found that along with progression of obesity-related diabetes, the H_2O_2 level was increased in the peripheral blood monocytes (Fig. 8E). Consistently, out data demonstrated that there was a negative relationship between relative FBW7 level and redox level of monocytes (Fig. 8F). Together, these data demonstrated that macrophage FBW7 expression is downregulated in obese patients and the lower FBW7 expression, the higher oxidative stress, inflammation and glucose level.

4. Discussion

In the present study, we have uncovered PKM2 as a novel bona fide ubiquitin substrate of SCF^{FBW7}. FBW7 targeted PKM2 for degradation in a ubiquitination-dependent manner. Importantly, we provided the evidence that FBW7 deficiency led to an increase in PKM2 level and activity, resulting in the inhibition of pentose phosphate pathway in macrophages, thus aggravating oxidative stress, inflammation response and insulin resistance in obesity. In addition, we also discovered that the expression of FBW7 in blood monocytes was highly negatively related with levels of ROS and inflammation in obesity.

The activities of many cellular proteins should be controlled both temporally and spatially, so that timely and appropriate deal could be achieved under various cellular stress responses. FBW7 balances physiological and pathological dysfunction by promoting the ubiquitination and degradation of various targets. The FBW7 gene locus encodes three isoforms (α, β and γ), and FBW7α is identified to perform most of the FBW7 functions, although specific roles for the other isoforms have also been described [38]. Interestingly, we found overexpression of FBW7 led to PKM2 instability, which was caused by the ubiquitin-proteasome system. Recently, Parkin were reported to interact with and ubiquitinate PKM2 in a Lys-186 and Lys-206 -linked manner [39]. Our data revealed that PKM2 is also a new target of FBW7, an E3 ubiquitin ligase. Through motif analysis and *in vitro* verification, we identified a perfectly CPD motif (S^{37}PAAS) in PKM2 for the ubiquitination by FBW7.

FBW7-mediated ubiquitination is required for the phosphorylation on the first threonine/serine in the CPD motif of some FBW7 target proteins [40]. The first Ser/Thr in the CPD motif could be phosphorylated by corresponding kinase, including Glycogen synthase kinase 3β (GSK3β), CDK1/2, or CDK5, and is important for substrate recognition by FBW7 [41,42]. GSK3β phosphorylated the great majority of FBW7 substrates, such as c-Jun, c-myc and CyclinE1 within their CPD motifs for recognition by FBW7 [42–44]. Unexpectedly, knockdown of GSK3β

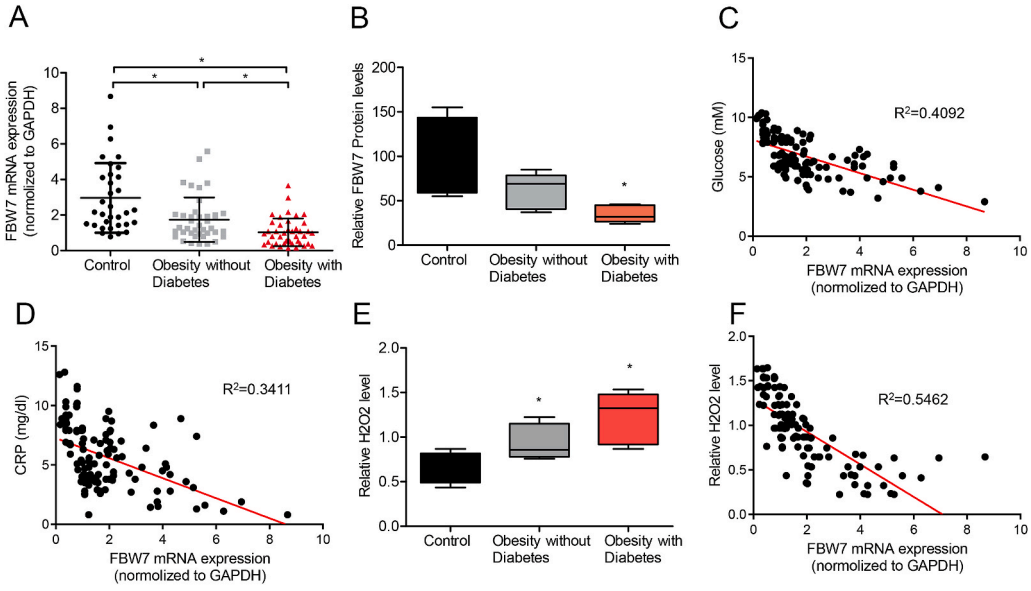

Fig. 8. FBW7 inversely correlates with the development of obesity-related diabetes.
(**A**) Relative FBW7 mRNA level was examined by real-time qPCR from human peripheral blood monocytes of obesity with or without diabetes, compared to the control volunteers. (**B**) The relative protein level of FBW7 in peripheral blood monocytes of obesity with or without diabetes compared to the control volunteers. (**C**) Correlation analysis between the glucose level and FBW7 mRNA level (normalized to GAPDH). $R^2 = 0.4092$, $P < 0.05$. (**D**) Correlation analysis between the CRP level and FBW7 mRNA level (normalized to GAPDH). $R^2 = 0.3411$, $P < 0.05$ (**E**) The relative H_2O_2 level in peripheral blood monocytes of obesity with or without diabetes compared to the control volunteers. (**F**) Correlation analysis between the relative H_2O_2 level and FBW7 mRNA level (normalized to GAPDH). $R^2 = 0.5462$, $P < 0.05$. Correlations was analyzed by Pearson's correlation coefficient analysis. Statistical significance was performed using two-tailed t-tests for two groups. $^*P < 0.05$ vs Control; $^{\#}P < 0.05$ vs Obesity without diabetes. All values are means ± SEM.

by siRNA could not attenuate the degradation of PKM2 by FBW7 (Fig. S6A), thus excluding the role of GSK3β in FBW7-mediated PKM2 ubiquitination. Maskey et al. reported that NDE1 could be phosphorylated by CDK5 within a specific FBW7 phosphodegron and degradation [45]. Consistently, our results showed knockdown of CDK5 by siRNA transfection could relieve the inhibition of FBW7 on PKM2 protein level (Fig. S6B). And co-overexpression of CDK5 could promote a dramatical decrease in the expression of wild-type PKM2, but not the PKM2 S37A mutant (Fig. S6C). Moreover, the dominant-negative mutant of CDK5 (CDK5 D145 N) had no effects on the PKM2 protein level compared with wild-type CDK5 (Fig. S6D). Collectively, it is possible that FBW7 ubiquitinates and targets pS37-PKM2 for proteasomal degradation in a CDK5-dependent manner. All these observations undercover the significance of precise regulation of PKM2 stability and related metabolic regulation in maintaining metabolic homeostasis.

Through the past decade, E3 ligase FBW7 has been demonstrated to participate in cell proliferation, angiogenesis, cell differentiation, tumor initiation and progression [16,41]. Previous researches reported that FBW7 regulated pro-inflammatory signaling by suppression of C/EBPδ expression for proteasomal degradation [17]. Here our work first revealed the essential roles of FBW7 in HFD-related metabolic dysfunction. Myeloid-specific FBW7 deficiency mice showed much more sensitivity to HFD-induced inflammation and insulin resistance. Deletion of FBW7 resulted in increased oxidative stress in macrophages when exposed to HFD or steric acids treatment. The direct consequence of redox activation was the obviously increased secretion of various cytokines, which could be blocked by the antioxidant NAC supplement. PKM2 acts as a bridge between the glycolysis and redox activation. However, Shira et al. reported that dimerized PKM2 translocated into nucleus, and induced proinflammatory reaction by phosphorylating tyrosine residues in STAT3 [46]. We then assessed STAT3 phosphorylation in the PMs from HFD-fed $FBW7^{fl/fl}Lysm^{Cre-/-}$ or $FBW7^{fl/fl}Lysm^{Cre+/-}$ mice. FBW7 deficiency in PMs clearly upregulated STAT3 phosphorylation at Y705 (Fig. S7). This result also suggested that the FBW7/PKM2/STAT3 axis might provide new opportunities for anti-inflammatory interventions in chronic metabolic disorder. Considering the SCF^{FBW7} complex is widely expressed in whole tissues, and promotes the ubiquitination and subsequent degradation of various proteins [47,48], multiple substrates of FBW7 may synergize and/or function to control the inflammatory homeostasis. Therefore, further studies are still needed to uncover the precise regulated network in FBW7-deficient macrophage during chronic inflammatory reaction.

PKM2 inhibition has been demonstrated to shunt glucose catabolism to PPP which plays a critical role in protecting against oxidative stress [22,49]. From our data, in FBW7 deficiency macrophages, high glycolysis combats the flow through the pentose phosphate pathway to inhibit ROS detoxification, thus aggravating the development of chronic inflammation and insulin resistance. It has been known that PKM2 switches between dimer and tetramer. Dimeric PKM2 with low pyruvate kinase activity can enter the nucleus, whereas tetrameric PKM2 has high activity in converting phosphoenolpyruvate to pyruvate [50]. Previous studies have identified that acute increases in intracellular ROS concentrations in human lung cancer cells caused inhibition of PKM2 through oxidation of Cys358. Oxidation of PKM2 inhibited its enzymatic activity via promoting dissociation of PKM2 subunits [22]. Although we found that FBW7 deletion could influence the expression and activity of PKM2, the detail mechanisms for the regulation of FBW7 on the structural dysfunction of PKM2 was still of interest to explore in the future.

In conclusion, our study identifies FBW7 as a negative regulator of PKM2, which drives macrophage metabolic switch and subsequently triggers redox protection in macrophages during obesity. These findings highlight the pivotal role for FBW7 in the obesity-related oxidative stress and inflammation, suggesting that macrophage FBW7 is novel potential strategy against obesity and insulin resistance.

Author contributions

C.W., K.H., and Y.L.C. designed the research studies. C.W., Y.L.C., W. J.X., Z.Y.L. and H.W. conducted experiments. C.W. and K.H. acquired and analyzed data. C.W. wrote the manuscript. All authors critically reviewed the manuscript.

Declaration of competing interest

The authors declare no competing financial or non-financial interests.

Acknowledgments

This work was supported by the National Natural Science Foundation of China (81900268, 81970257, 81830014), Major Program of National Natural Science Foundation of China (91949201), and Ministry of Science and Technology of China (2016 YFA0101100).

Appendix A. Supplementary data

Supplementary data to this article can be found online at https://doi.org/10.1016/j.redox.2020.101688.

References

[1] U.J. Jung, M.S. Choi, Obesity and its metabolic complications: the role of adipokines and the relationship between obesity, inflammation, insulin resistance, dyslipidemia and nonalcoholic fatty liver disease, Int. J. Mol. Sci. 15 (4) (2014) 6184–6223. Epub 2014/04/16.
[2] A.R. Saltiel, J.M. Olefsky, Inflammatory mechanisms linking obesity and metabolic disease, J. Clin. Invest. 127 (1) (2017) 1–4.
[3] A. Chawla, K.D. Nguyen, Y.P. Goh, Macrophage-mediated inflammation in metabolic disease, Nat. Rev. Immunol. 11 (11) (2011) 738–749.
[4] H. Shapiro, A. Lutaty, A. Ariel, Macrophages, meta-inflammation, and immunometabolism, ScientificWorldJournal 11 (2011) 2509–2529.
[5] K. Makki, P. Froguel, I. Wolowczuk, Adipose tissue in obesity-related inflammation and insulin resistance: cells, cytokines, and chemokines, ISRN Inflamm 2013 (2013) 139239.
[6] Y.C. Liu, X.B. Zou, Y.F. Chai, Y.M. Yao, Macrophage polarization in inflammatory diseases, Int. J. Biol. Sci. 10 (5) (2014) 520–529.
[7] K. Yumimoto, M. Matsumoto, I. Onoyama, K. Imaizumi, K.I. Nakayama, F-box and WD repeat domain-containing-7 (Fbxw7) protein targets endoplasmic reticulum-anchored osteogenic and chondrogenic transcriptional factors for degradation, J. Biol. Chem. 288 (40) (2013) 28488–28502.
[8] M. Gorelik, S. Orlicky, M.A. Sartori, X. Tang, E. Marcon, I. Kurinov, et al., Inhibition of SCF ubiquitin ligases by engineered ubiquitin variants that target the Cul1 binding site on the Skp1-F-box interface, Proc. Natl. Acad. Sci. U. S. A. 113 (13) (2016) 3527–3532.
[9] B. Hao, S. Oehlmann, M.E. Sowa, J.W. Harper, N.P. Pavletich, Structure of a Fbw7-Skp1-cyclin E complex: multisite-phosphorylated substrate recognition by SCF ubiquitin ligases, Mol. Cell. 26 (1) (2007) 131–143.
[10] J. O'Neil, J. Grim, P. Strack, S. Rao, D. Tibbitts, C. Winter, et al., FBW7 mutations in leukemic cells mediate NOTCH pathway activation and resistance to gamma-secretase inhibitors, J. Exp. Med. 204 (8) (2007) 1813–1824.
[11] M. Welcker, A. Orian, J.E. Grim, R.N. Eisenman, B.E. Clurman, A nucleolar isoform of the Fbw7 ubiquitin ligase regulates c-Myc and cell size, Curr. Biol. 14 (20) (2004) 1852–1857.
[12] J. Zhao, X. Xiong, Y. Li, X. Liu, T. Wang, H. Zhang, et al., Hepatic F-box protein FBXW7 maintains glucose homeostasis through degradation of fetuin-A, Diabetes 67 (5) (2018) 818–830.
[13] J.D. Hoeck, A. Jandke, S.M. Blake, E. Nye, B. Spencer-Dene, S. Brandner, et al., Fbw7 controls neural stem cell differentiation and progenitor apoptosis via Notch and c-Jun, Nat. Neurosci. 13 (11) (2010) 1365–1372.
[14] R. Wang, Y. Wang, N. Liu, C. Ren, C. Jiang, K. Zhang, et al., FBW7 regulates endothelial functions by targeting KLF2 for ubiquitination and degradation, Cell Res. 23 (6) (2013) 803–819.
[15] I. Onoyama, A. Suzuki, A. Matsumoto, K. Tomita, H. Katagiri, Y. Oike, et al., Fbxw7 regulates lipid metabolism and cell fate decisions in the mouse liver, J. Clin. Invest. 121 (1) (2011) 342–354.
[16] Y. Song, L. Lai, Z. Chong, J. He, Y. Zhang, Y. Xue, et al., E3 ligase FBXW7 is critical for RIG-I stabilization during antiviral responses, Nat. Commun. 8 (2017) 14654.
[17] K. Balamurugan, S. Sharan, K.D. Klarmann, Y. Zhang, V. Coppola, G.H. Summers, et al., FBXW7alpha attenuates inflammatory signalling by downregulating C/EBPdelta and its target gene Tlr4, Nat. Commun. 4 (2013) 1662. Epub 2013/04/12.

[18] M.T. Bengoechea-Alonso, J. Ericsson, The ubiquitin ligase Fbxw7 controls adipocyte differentiation by targeting C/EBPalpha for degradation, Proc. Natl. Acad. Sci. U.S.A. 107 (26) (2010) 11817–11822. Epub 2010/06/11.
[19] S. Sun, Y. Ji, S. Kersten, L. Qi, Mechanisms of inflammatory responses in obese adipose tissue, Annu. Rev. Nutr. 32 (2012) 261–286.
[20] C. de Luca, J.M. Olefsky, Inflammation and insulin resistance, FEBS Lett. 582 (1) (2008) 97–105. Epub 2007/12/07.
[21] G. Verdile, K.N. Keane, V.F. Cruzat, S. Medic, M. Sabale, J. Rowles, et al., Inflammation and oxidative stress: the molecular connectivity between insulin resistance, obesity, and alzheimer's disease, Mediat. Inflamm. 2015 (2015) 105828. Epub 2015/12/23.
[22] S. Tangvarasittichai, Oxidative stress, insulin resistance, dyslipidemia and type 2 diabetes mellitus, World J. Diabetes 6 (3) (2015) 456–480. Epub 2015/04/22.
[23] V. Ormazabal, S. Nair, O. Elfeky, C. Aguayo, C. Salomon, F.A. Zuniga, Association between insulin resistance and the development of cardiovascular disease, Cardiovasc. Diabetol. 17 (1) (2018) 122. Epub 2018/09/02.
[24] A. Viola, F. Munari, R. Sanchez-Rodriguez, T. Scolaro, A. Castegna, The metabolic signature of macrophage responses, Front. Immunol. 10 (2019) 1462. Epub 2019/07/25.
[25] C. Diskin, E.M. Palsson-McDermott, Metabolic modulation in macrophage effector function, Front. Immunol. 9 (2018) 270. Epub 2018/03/10.
[26] J.C. Alves-Filho, E.M. Palsson-McDermott, Pyruvate kinase M2: a potential target for regulating inflammation, Front. Immunol. 7 (2016) 145. Epub 2016/05/06.
[27] D. Anastasiou, G. Poulogiannis, J.M. Asara, M.B. Boxer, J.K. Jiang, M. Shen, et al., Inhibition of pyruvate kinase M2 by reactive oxygen species contributes to cellular antioxidant responses, Science 334 (6060) (2011) 1278–1283. Epub 2011/11/05.
[28] E. Mullarky, L.C. Cantley, Diverting glycolysis to combat oxidative stress, in: K. Nakao, N. Minato, S. Uemoto (Eds.), Innovative Medicine: Basic Research and Development. Tokyo, 2015, pp. 3–23.
[29] C. Wang, W. Xu, J. An, M. Liang, Y. Li, F. Zhang, et al., Poly(ADP-ribose) polymerase 1 accelerates vascular calcification by upregulating Runx2, Nat. Commun. 10 (1) (2019) 1203. Epub 2019/03/15.
[30] C. Wang, W. Xu, Y. Zhang, F. Zhang, K. Huang, PARP1 promote autophagy in cardiomyocytes via modulating FoxO3a transcription, Cell Death Dis. 9 (11) (2018) 1047.
[31] M.H. Barros, F. Hauck, J.H. Dreyer, B. Kempkes, G. Niedobitek, Macrophage polarisation: an immunohistochemical approach for identifying M1 and M2 macrophages, PloS One 8 (11) (2013), e80908. Epub 2013/11/22.
[32] Y. Bai, Q. Sun, Macrophage recruitment in obese adipose tissue, Obes. Rev. 16 (2) (2015) 127–136.
[33] R.E. Lamb, B.J. Goldstein, Modulating an oxidative-inflammatory cascade: potential new treatment strategy for improving glucose metabolism, insulin resistance, and vascular function, Int. J. Clin. Pract. 62 (7) (2008) 1087–1095. Epub 2008/05/21.
[34] H. Lan, M. Tan, Q. Zhang, F. Yang, S. Wang, H. Li, et al., LSD1 destabilizes FBXW7 and abrogates FBXW7 functions independent of its demethylase activity, Proc. Natl. Acad. Sci. U.S.A. 116 (25) (2019) 12311–12320. Epub 2019/06/04.
[35] S. Dikalov, Cross talk between mitochondria and NADPH oxidases, Free Radic. Biol. Med. 51 (7) (2011) 1289–1301. Epub 2011/07/23.
[36] J. Chen, J. Xie, Z. Jiang, B. Wang, Y. Wang, X. Hu, Shikonin and its analogs inhibit cancer cell glycolysis by targeting tumor pyruvate kinase-M2, Oncogene 30 (42) (2011) 4297–4306. Epub 2011/04/26.
[37] M.G. Vander Heiden, H.R. Christofk, E. Schuman, A.O. Subtelny, H. Sharfi, E. E. Harlow, et al., Identification of small molecule inhibitors of pyruvate kinase M2, Biochem. Pharmacol. 79 (8) (2010) 1118–1124. Epub 2009/12/17.
[38] J. Cao, M.H. Ge, Z.Q. Ling, Fbxw7 tumor suppressor: a vital regulator contributes to human tumorigenesis, Medicine (Baltim.) 95 (7) (2016), e2496.
[39] K. Liu, F. Li, H. Han, Y. Chen, Z. Mao, J. Luo, et al., Parkin regulates the activity of pyruvate kinase M2, J. Biol. Chem. 291 (19) (2016) 10307–10317.
[40] R.J. Davis, M. Welcker, B.E. Clurman, Tumor suppression by the Fbw7 ubiquitin ligase: mechanisms and opportunities, Canc. Cell 26 (4) (2014) 455–464.
[41] D. Flugel, A. Gorlach, T. Kietzmann, GSK-3beta regulates cell growth, migration, and angiogenesis via Fbw7 and USP28-dependent degradation of HIF-1alpha, Blood 119 (5) (2012) 1292–1301.
[42] M. Welcker, A. Orian, J. Jin, J.E. Grim, J.W. Harper, R.N. Eisenman, et al., The Fbw7 tumor suppressor regulates glycogen synthase kinase 3 phosphorylation-dependent c-Myc protein degradation, Proc. Natl. Acad. Sci. U. S. A. 101 (24) (2004) 9085–9090.
[43] R. Babaei-Jadidi, N. Li, A. Saadeddin, B. Spencer-Dene, A. Jandke, B. Muhammad, et al., FBXW7 influences murine intestinal homeostasis and cancer, targeting Notch, Jun, and DEK for degradation, J. Exp. Med. 208 (2) (2011) 295–312.
[44] X. Ye, G. Nalepa, M. Welcker, B.M. Kessler, E. Spooner, J. Qin, et al., Recognition of phosphodegron motifs in human cyclin E by the SCF(Fbw7) ubiquitin ligase, J. Biol. Chem. 279 (48) (2004) 50110–50119.
[45] D. Maskey, M.C. Marlin, S. Kim, S. Kim, E.C. Ong, G. Li, et al., Cell cycle-dependent ubiquitylation and destruction of NDE1 by CDK5-FBW7 regulates ciliary length, EMBO J. 34 (19) (2015) 2424–2440.
[46] T. Shirai, R.R. Nazarewicz, B.B. Wallis, R.E. Yanes, R. Watanabe, M. Hilhorst, et al., The glycolytic enzyme PKM2 bridges metabolic and inflammatory dysfunction in coronary artery disease, J. Exp. Med. 213 (3) (2016) 337–354. Epub 2016/03/02.
[47] K.M. Crusio, B. King, L.B. Reavie, I. Aifantis, The ubiquitous nature of cancer: the role of the SCF(Fbw7) complex in development and transformation, Oncogene 29 (35) (2010) 4865–4873. Epub 2010/06/15.
[48] K. Shimizu, N.T. Nihira, H. Inuzuka, W. Wei, Physiological functions of FBW7 in cancer and metabolism, Cell. Signal. 46 (2018) 15–22. Epub 2018/02/24.
[49] M. Siragusa, J. Thole, S.I. Bibli, B. Luck, A.E. Loot, K. de Silva, et al., Nitric oxide maintains endothelial redox homeostasis through PKM2 inhibition, EMBO J. 38 (17) (2019), e100938. Epub 2019/07/23.
[50] K. Zahra, T. Dey, Ashish, S.P. Mishra, U. Pandey, Pyruvate kinase M2 and cancer: the role of PKM2 in promoting tumorigenesis, Frontiers in oncology 10 (2020) 159. Epub 2020/03/21.